JACS
JOURNAL OF THE AMERICAN CHEMICAL SOCIETY

Communication

pubs.acs.org/JACS

Ordered Mesoporous Black TiO_2 as Highly Efficient Hydrogen Evolution Photocatalyst

Wei Zhou,[†,‡] Wei Li,[§,‡] Jian-Qiang Wang,[#] Yang Qu,[†] Ying Yang,[†] Ying Xie,[†] Kaifu Zhang,[†] Lei Wang,[†] Honggang Fu,*[,†] and Dongyuan Zhao*[,§]

[†]Key Laboratory of Functional Inorganic Material Chemistry, Ministry of Education of the People's Republic of China, Heilongjiang University, Harbin 150080, P. R. China

[§]Department of Chemistry, Laboratory of Advanced Materials, Shanghai Key Lab of Molecular Catalysis and Innovative Materials, and State Key Laboratory of Molecular Engineering of Polymers, Fudan University, Shanghai 200433, P. R. China

[#]Shanghai Synchrotron Radiation Facility (SSRF), Shanghai Institute of Applied Physics, Chinese Academy of Sciences, Shanghai 201204, P. R. China

Supporting Information

ABSTRACT: Mesoporous TiO_2 has gained increasing interest because of its outstanding properties and promising applications in a wide range of fields. Herein, we report the facile synthesis of ordered mesoporous black TiO_2 (OMBT) materials, which exhibit excellent photocatalytic hydrogen evolution performances. In this case, the employment of a thermally stable and high-surface-area mesoporous TiO_2 as the hydrogenation precursor is the key for fabricating the OMBT materials, which not only facilitate H_2 gas diffusion into TiO_2 and interaction with their structures but also maintain the ordered mesoporous structures as well as inhibit the phase transformation (from anatase to rutile) and crystal growth during hydrogenation at 500 °C. The resultant OMBT materials possess a relatively high surface area of ~124 $m^2\ g^{-1}$ and a large pore size and pore volume of ~9.6 nm and 0.24 $cm^3\ g^{-1}$, respectively. More importantly, the OMBT materials can extend the photoresponse from ultraviolet to visible and infrared light regions and exhibit a high solar-driven hydrogen production rate (136.2 μmol h^{-1}), which is almost two times as high as that of pristine mesoporous TiO_2 (76.6 μmol h^{-1}).

Mesoporous TiO_2 materials with interpenetrated and regular mesopore systems have recently triggered enormous research activities because of their fascinating features such as low cost, environmental benignity, good chemical stability, excellent electronic and optical properties, high specific surface areas, tunable mesostructures and pore sizes.[1] While they possess great potential in photocatalysis, photoelectrochemical (PEC) water splitting, and photovoltaic (PV) cells, it is more intriguing to explore the possibility of enhancing and/or extending their properties by increasing the solar-light adsorption and improving the charge separation and transportation.[2] Until this date, numerous efforts involving engineering bandgap, maximizing crystallinity, optimizing exposed facets and controlling heterojunctions have been carried out worldwide to design and pursue high-performance mesoporous TiO_2 materials.[3]

Recently, Mao and co-workers have demonstrated a novel approach to enhance the solar harvesting by introducing disorder in the surface layers of high crystalline TiO_2 nanoparticles through hydrogenation.[4] The resultant hydrogenated TiO_2 nanocrystals showed the optical absorption shifts from the regions ultraviolet (UV) to near-infrared, accompanied by a dramatic color change from white to black. As a result, a great improvement of the photocatalytic performance was obtained. Since then, much work has been devoted to the synthesis and design of black TiO_2 materials, which truly represent a big breakthrough in the photocatalytic splitting.[5] However, the mostly investigated black TiO_2 materials usually possess a poorly porous structure with limited surface areas of lower than 50 $m^2\ g^{-1}$, which are generally composed of irregular nanoparticles.

Herein, we demonstrate, for the first time, the facile synthesis of mesoporous black TiO_2 with an ordered mesostructure, high surface areas, and highly crystalline anatase pore walls. A thermally stable and high-surface-area mesoporous TiO_2 (OMT) was first fabricated via an evaporation-induced self-assembly (EISA) method combined with an ethylenediamine encircling process, which was selected as the precursor for the subsequent hydrogenation (Figure 1). The resultant ordered mesoporous black TiO_2 (OMBT) materials possess a relatively high surface area of ~124 $m^2\ g^{-1}$ and a large pore size and pore volume of ~9.6 nm and 0.24 $cm^3\ g^{-1}$, respectively. More importantly, the OMBT materials can extend the photoresponse from UV light to visible and infrared light regions and exhibit a very high photocatalytic hydrogen generation rate of 136.2 μmol h^{-1}, which is almost two times as high as that of pristine OMT (76.6 μmol h^{-1}).

After hydrogenation at 500 °C, the X-ray diffraction (XRD) pattern of the OMBT materials (Figure S1A) still shows well-defined diffraction peaks of anatase phase but a larger line-width than that of pristine OMT, combined with a dramatic color change from white to black (Figure S1B). These results clearly reveal the structure stability of OMT materials and successful surface disordered engineering of high crystalline anatase nanoparticles during the H_2 annealing treatment.[5] The structural

Received: May 14, 2014
Published: June 17, 2014

dx.doi.org/10.1021/ja504802q | J. Am. Chem. Soc. 2014, 136, 9280−9283

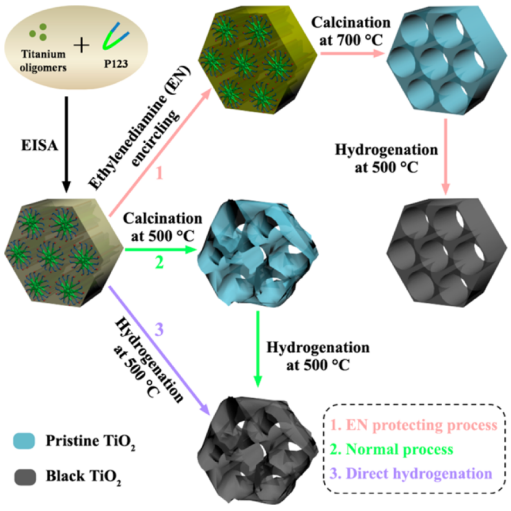

Figure 1. Schematic synthesis process for the ordered mesoporous black TiO_2 materials.

changes of OMBT materials after the introduction of disordered components were further investigated by Raman spectroscopy (Figure S2). Four peaks at 149.3, 397.5, 515.1, and 639.0 cm^{-1} are observed in the OMBT materials (Figure S2), which can be well assigned into typical anatase Raman bands of E_g, B_{1g}, A_{1g}, E_g, respectively. The obvious shifting and broadening of these peaks further demonstrate that the original symmetry of TiO_2 lattice is broken down due to the disordered surface after the hydrogen annealing process.[5]

Transmission electron microscopy (TEM) images (Figure 2a,b) of the OMBT materials viewed along the [001] and [110]

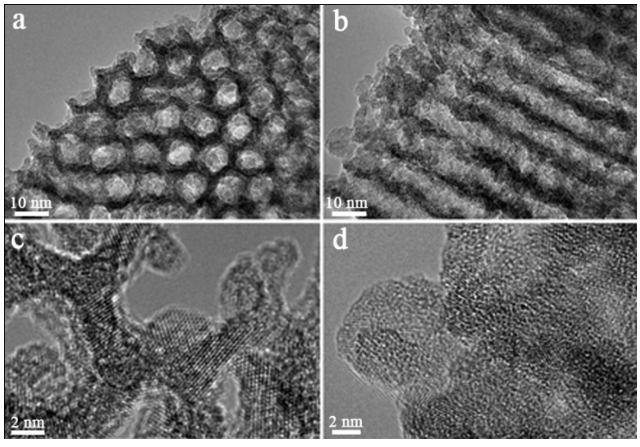

Figure 2. Representative TEM images along (a) [100] and (b) [110] planes and (c,d) HRTEM images of the ordered mesoporous black TiO_2 materials after hydrogen gas annealing at 500 °C.

directions show well-ordered hexagonal arrays of mesopores with a *p6mm* symmetry, indicating that a two-dimensional (2D) ordered hexagonal mesostructure can be well retained after the high-temperature H_2 annealing treatment, which was further demonstrated by the low-angle XRD patterns (Figure S3). The average pore size and wall thickness is about 9 and 5 nm, respectively. The large domain regularity of the OMBT materials is further verified by TEM images (Figure S4A). HRTEM images (Figure 2c,d) clearly show that the mesopore walls are consisted by highly crystalline TiO_2 nanoparticles. A well-defined crystalline lattice can be identified with a *d*-spacing of 0.35 nm corresponding to the (101) plane of anatase TiO_2.[6] The high crystallinity can also be confirmed by the selected-area electron diffraction pattern image (Figure S4B). Moreover, a thin disordered surface layer coating on a crystalline core can also be clearly appreciated, further indicating the successful hydrogenation.

N_2 adsorption/desorption isotherms (Figure S5A) of the OMBT materials before and after hydrogenation both show typical type IV curves with a sharp capillary condensation step at P/P_0 = 0.8−0.9 and an H1-type hysteresis loop, which is typical of large-pore mesoporous materials with cylindrical channels. The Brunauer−Emmett−Teller surface area and pore volume of the OMBT materials are calculated to be as high as ~124 $m^2\ g^{-1}$ and 0.24 $cm^3\ g^{-1}$, respectively. The pore size derived from the adsorption branches of the isotherms by using the Barrett−Joyner−Halenda method is about 9.6 nm with a narrow distribution (Figure S5B). All the data are comparable with those of pristine OMT (Table S1), indicating that mesostructures can be well retained during the high-temperature H_2 annealing treatment, consistent with the observations of TEM results discussed above.

The absorption spectra (Figure S6A) show that the OMBT materials can extend the photoresponse from UV light to visible and infrared light regions. The bandgap of the OMBT materials is measured to be about 2.82 eV, smaller than that of pristine OMT (~3.15 eV) (Figure S6B). As demonstrated previously, it may be attributed to the formation of Ti^{3+} in the surface disordered layer. X-ray photoelectron spectroscopy (XPS) (Figure S7) and X-ray absorption fine structure spectroscopy (XAFS) (Figure 3) were used to investigate the chemical binding

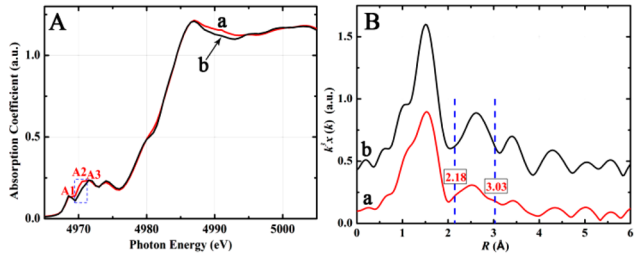

Figure 3. Normalized X-ray absorption near-edge structure (A) and normalized Fourier transforms of the extended X-ray absorption fine structure spectra (B) for the ordered mesoporous black TiO_2 materials (a) and pristine ordered mesoporous TiO_2 materials (b) at the Ti K-edge. The A1 prepeak is owing to t_{2g} band-like state, while A2 and A3 are due to e_g band-like states.

and valence band position of the OMBT materials before and after hydrogenation. The Ti 2p spectra (Figure S6A) are almost identical for both OMBT and pristine OMT materials with TiO_2 peaks centered at binding energies of 458.5 and 464.4 eV, which are typical for the Ti^{4+} species in TiO_2. The O 1s spectra of the OMBT and pristine OMT materials show dramatic differences (Figure S7B). The OMBT exhibits a broader O 1s peak with a strong shoulder at high binding energy, which can be deconvoluted into two peaks centered at 530.1 and 531.6 eV. The broader peak at 531.6 eV could be attributed to Ti−OH species, implying the formation of hydroxyl groups on TiO_2 surface after hydrogenation.[5] The valence band XPS for OMT displays typical valence band characteristics of anatase TiO_2, with the edge of the maximum energy at about 1.95 eV (Figure S7C). While the valence band maximum energy for OMBT blue-shifts toward to the vacuum level at ~1.60 eV, further indicating the

dx.doi.org/10.1021/ja504802q | J. Am. Chem. Soc. 2014, 136, 9280−9283

efficient surface hydrogenation. The intensity of the Ti K-edge pre-edge transitions is sensitive to the symmetry of the surrounding atoms, being dipole forbidden, which would increase as the environment is distorted.[7] The enhanced intensity (Figure 3A) combined with the increased Debye−Waller factor (Table S2) verifies the existence of distorted structures in the OMBT materials. In addition, the A2 prepeak shifts to low-energy, while the A1 prepeak shifts to high-energy (Figure 3A), indicating that the crystal field split energy (Δ) of Ti 3d reduces. It confirms the formation of low valence Ti on the basis of its weak cationic polarization for O^{2-}.[7] Obviously, two new peaks of the OMBT materials at 2.18 and 3.03 Å can be clearly appreciated from the normalized Fourier transforms of the EXAFS spectra (Figure 3B), which can be attributed to Ti_2O_3. Moreover, the coordination number of Ti−Ti and Ti−O in the OMBT materials is quite similar to that of Ti_2O_3 (Table S2), further confirming the existence of Ti^{3+}.[7]

To validate the role of the ethylenediamine encircling processs, a set of control experiments were conducted. In the absence of ethylenediamine protecting (Figure 1, route 2), the ordered mesoporous structure collapsed when the as-made mesophase was treated by heating at 500 °C for full conversion to crystalline state and removal of surfactants (Figure S8). Followed by hydrogenation at 500 °C, the porous structure further decayed combined with a partial phase transformation from anatase to rutile owing to the intrinsic crystal growth and sintering induced by high temperature (Figure S9). On the other hand, the as-made mesophase was directly hydrogenated at 500 °C (Figure 1, route 3), which also resulted in a disordered mesoporous TiO_2 with a mixed phase and a low surface area of ∼62 m^2 g^{-1} (Figure S10, Table S1) due to the low thermal stability. In this case, by using the ethylenediamine protecting strategy (Figure 1, route 1), high crystalline ordered mesoporous anatase with a well-ordered mesostructure, a high surface area and a large pore size can be facilely obtained, which can be stabilized up to 800 °C owing to the presence of surface bonded N-containing species.[3f] That makes them an promising candidate for OMBT materials. Because it can not only facilitate H_2 gas diffusion into TiO_2 and interaction with its structure, but also retain the ordered mesoporous structures, as well as inhibit the phase transformation (from anatase to rutile) and crystal growth during the high-temperature H_2 gas annealing (at 500 °C), even if it has been found that the temperature of anatase to rutile phase transition drops to 500 °C under H_2 gas.[5b]

The OMBT materials were evaluated as the H_2 evolution photocatalysts and showed a much higher photocatalytic activity with a reaction rate of 136.2 μmol h^{-1} than that of the pristine OMT materials (76.6 μmol h^{-1}) under AM 1.5 (Figure 4A) with a power density of 100 mW/cm^2 based on 100 mg of the catalyst. No noticeable decrease in H_2 production rate for both OMBT and OMT materials in 10 cycling tests were observed within the 30 h photocatalytic period (the reactor was replenished with 1 mL of methanol and degassed in vacuum before each cycling test), which indicating their high stability and photocatalytic activity throughout the testing cycles. Moreover, it further eliminates the possibility that black TiO_2 photocatalysts act as a hydrogen reservoir in these experiments.[4] By filtering out incident light with wavelengths shorter than about 400 nm (Figure S11), the OMBT materials still exhibited a very good photocatalytic activity. The hydrogen generation rate of the OMBT materials at 365 nm is 68 μmol h^{-1}, which is much larger than that at 420 (0.9 μmol h^{-1}) and 520 nm (0.44 μmol h^{-1}) (Figure 4B). It indicates that UV light is the main contributor to

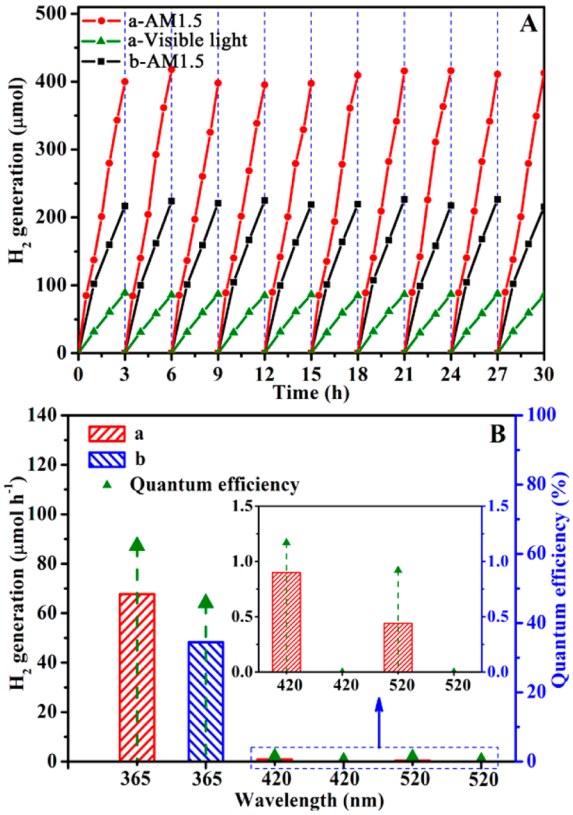

Figure 4. Photocatalytic hydrogen evolution of the ordered mesoporous black TiO_2 (a) and pristine ordered mesoporous TiO_2 materials (b). (A) Cycling tests of photocatalytic hydrogen generation under AM 1.5 and visible light irradiation. (B) The photocatalytic hydrogen evolution rates under single-wavelength light and the corresponding QE. The inset enlarges the QE of single-wavelength light at 420 and 520 nm.

the high photocatalytic activity of the OMBT materials under AM 1.5. As a control, no H_2 can be detected for the OMT materials under visible light irradiation, further demonstrating that the hydrogenation process could effectively promote the photocatalytic activities of mesoporous TiO_2 under both UV and visible light. Moreover, without Pt as a cocatalyst or methanol as a sacrificial agent, the OMBT materials still show superior photocatalytic performances to OMT materials, even both the hydrogen production rates are ultralow (Figure S12). In addition, to testify the solar energy conversion efficiency, apparent quantum efficiency (QE) for different single wavelengths was measured to be 62.3 and 45.8% for the OMBT and OMT materials at 365 nm, respectively, implying the high utilization ratio of photogenerated charges. In visible light region, the QE of the OMBT materials is still up to ∼1%. The efficient separation of photogenerated charges of the OMBT materials was further demonstrated by the surface photovoltage spectroscopy (SPS) analysis (Figure S13A). Compared to OMT materials, the onset of the OMBT materials is red-shifted, suggesting the visible light photoactive. Moreover, after the high-temperature hydrogenation, the lifetime of photogenerated charges is greatly prolonged according to transient-state surface photovoltage spectra (Figure S13B), which further offers evidence for the high photocatalytic hydrogen generation of the OMBT materials.

The photoelectrochemical properties of the OMBT materials were also performed. Linear sweeps voltammogram of the OMBT materials shows a photocurrent density of 68 μA cm^{-2},

dx.doi.org/10.1021/ja504802q | J. Am. Chem. Soc. 2014, 136, 9280−9283

which is almost four times as high as that of the OMT materials (18 μA cm^{-2}) under AM 1.5 (Figure 5A). The chronoamperometry responses of both OMBT and OMT materials at 0.8 V are constant (Figure 5B), indicating their good stabilities. The electrochemical impedance measurements show smaller interfacial resistance for the OMBT materials than that of OMT, indicating a more efficient charge separation (Figure 5C). Both samples showed a positive slope in the Mott–Schottky plots, as expected for *n*-type semiconductors (Figure 5D). The OMBT materials showed a substantially smaller slope of the Mott–Schottky plot than the OMT materials, suggesting an increase of donor density due to the presence of Ti^{3+} on the surface disordered layer.[5a−d] That may be responsible for the high photocatalytic activities of the OMBT materials.

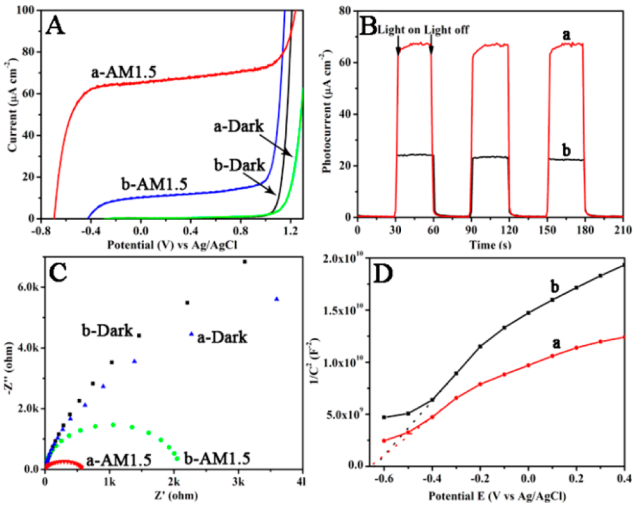

Figure 5. Photoelectrochemical properties of the ordered mesoporous black TiO_2 materials (a) and pristine ordered mesoporous TiO_2 materials (b): (A) Linear sweeps voltammograms under dark and AM 1.5, (B) the chronoamperometry, (C) the Nyquist plots of electrochemical impedance under dark and AM 1.5, and (D) the Mott–Schottky plots.

In conclusion, we have demonstrated a facile synthesis of mesoporous black TiO_2 materials with a highly ordered hexagonal mesostructure, a relatively high surface area of ~124 m^2 g^{-1}, and a large pore size and pore volume of ~9.6 nm and 0.24 cm^3 g^{-1}, respectively. We have found that the employment of a thermally stable and high-surface-area mesoporous TiO_2 as the hydrogenation precursor is key for fabricating the OMBT materials, which not only facilitate H_2 gas diffusion into TiO_2 and interaction with its structure but also retain the ordered mesoporous structures as well as inhibit the phase transformation (from anatase to rutile) and crystal growth during hydrogenation at 500 °C. The resultant OMBT materials show an extended photoresponse from UV light to visible and infrared light regions, as a result, exhibiting a very high photocatalytic hydrogen evolution rate of 136.2 μmol h^{-1}, which is almost two times as high as that of pristine OMT (76.6 μmol h^{-1}).

■ ASSOCIATED CONTENT

Ⓢ Supporting Information

Experimental procedures and data. This material is available free of charge via the Internet at http://pubs.acs.org.

■ AUTHOR INFORMATION

Corresponding Author

dyzhao@fudan.edu.cn; fuhg@vip.sina.com

Author Contributions

‡These authors contributed equally.

Notes

The authors declare no competing financial interest.

■ ACKNOWLEDGMENTS

We gratefully acknowledge the support of State Key Basic Research Program (2013CB934104), the Key Program Projects of the National Natural Science Foundation of China (21031001, 21210004), the National Natural Science Foundation of China (91122018, 21371053, 21376065), the Cultivation Fund of the Key Scientific and Technical Innovation Project, Ministry of Education of China (708029).

■ REFERENCES

(1) (a) Yang, P.; Zhao, D.; Margolese, D. I.; Chmelka, B. F.; Stucky, G. D. *Nature* **1998**, *396*, 152. (b) Ivanova, A.; Fattakhova-Rohlfing, D.; Kayaalp, B. E.; Rathouský, J.; Bein, T. *J. Am. Chem. Soc.* **2014**, *136*, 5930. (c) Crossland, E. J. W.; Noel, N.; Sivaram, V.; Leijtens, T.; Alexander-Webber, J. A.; Snaith, H. J. *Nature* **2013**, *495*, 215. (d) Bian, Z.; Tachikawa, T.; Zhang, P.; Fujitsuka, M.; Majima, T. *J. Am. Chem. Soc.* **2013**, *136*, 458.

(2) (a) Li, W.; Wu, Z.; Wang, J.; Elzatahry, A. A.; Zhao, D. *Chem. Mater.* **2014**, *26*, 287. (b) Zhou, W.; Fu, H. *ChemCatChem* **2013**, *5*, 885. (c) Vivero-Escoto, J. L.; Chiang, Y. D.; C-Wwu, K.; Yamauchi, Y. *Sci. Technol. Adv. Mater.* **2012**, *13*, 013003.

(3) (a) Li, H.; Bian, Z.; Zhu, J.; Huo, Y.; Li, H.; Lu, Y. *J. Am. Chem. Soc.* **2007**, *129*, 4538. (b) Liu, G.; Zhao, Y.; Sun, C.; Li, F.; Lu, G. Q.; Cheng, H. M. *Angew. Chem., Int. Ed.* **2008**, *47*, 4516. (c) Lee, J.; Christopher, O. M.; Warren, S. C.; Kamperman, M.; DiSalvo, F. J.; Wiesner, U. *Nat. Mater.* **2008**, *7*, 222. (d) Zhang, R.; Tu, B.; Zhao, D. *Chem.—Eur. J.* **2010**, *16*, 9977. (e) Bian, Z.; Zhu, J.; Wen, J.; Cao, F.; Huo, Y.; Qian, X.; Cao, Y.; Shen, M.; Li, H.; Lu, Y. *Angew. Chem., Int. Ed.* **2011**, *50*, 1105. (f) Zhou, W.; Sun, F.; Pan, K.; Tian, G.; Jiang, B.; Ren, Z.; Tian, C.; Fu, H. *Adv. Funct. Mater.* **2011**, *21*, 1922. (g) Joo, J. B.; Zhang, Q.; Lee, I.; Dahl, M.; Zaera, F.; Yin, Y. *Adv. Funct. Mater.* **2012**, *22*, 166.

(4) Chen, X.; Liu, L.; Yu, P. Y.; Mao, S. S. *Science* **2011**, *331*, 746.

(5) (a) Wang, Z.; Yang, C. Y.; Lin, T. Q.; Yin, H.; Chen, P.; Wan, D. Y.; Xu, F. F.; Huang, F. Q.; Lin, J. H.; Xie, X. M.; Jiang, M. H. *Adv. Funct. Mater.* **2013**, *23*, 5444. (b) Naldoni, A.; Allieta, M.; Santangelo, S.; Marelli, M.; Fabbri, F.; Cappelli, S.; Bianchi, C. L.; Psaro, R.; Dal Santo, V. *J. Am. Chem. Soc.* **2012**, *134*, 7600. (c) Chen, X.; Liu, L.; Liu, Z.; Marcus, M. A.; Wang, W.-C.; Oyler, N. A.; Grass, M. E.; Mao, B.; Glans, P.-A.; Yu, P. Y.; Guo, J.; Mao, S. S. *Sci. Rep.* **2013**, *3*, 1510. (d) Wang, Z.; Yang, C. Y.; Lin, T. Q.; Yin, H.; Chen, P.; Wan, D. Y.; Xu, F. F.; Huang, F. Q.; Lin, J. H.; Xie, X. M.; Jiang, M. H. *Energy Environ. Sci.* **2013**, *6*, 3007. (e) Yang, C. Y.; Wang, Z.; Lin, T. Q.; Yin, H.; Lu, X. J.; Wan, D. Y.; Xu, T.; Zheng, C.; Lin, J. H.; Huang, F. Q.; Xie, X. M.; Jiangl, M. H. *J. Am. Chem. Soc.* **2013**, *135*, 17831. (f) Zheng, Z.; Huang, B.; Lu, J.; Wang, Z.; Qin, X.; Zhang, X.; Dai, Y.; Whangbo, M.-H. *Chem. Commun.* **2012**, *48*, 5733. (g) Wang, G. M.; Wang, H. Y.; Ling, Y. C.; Tang, Y. C.; Yang, X. Y.; Fitzmorris, R. C.; Wang, C. C.; Zhang, J. Z.; Li, Y. *Nano Lett.* **2011**, *11*, 3026.

(6) Li, W.; Wang, F.; Feng, S.; Wang, J.; Sun, Z.; Li, B.; Li, Y.; Yang, J.; Elzatahry, A. A.; Xia, Y.; Zhao, D. *J. Am. Chem. Soc.* **2013**, *135*, 18300.

(7) (a) Luca, V.; Djajanti, S.; Howe, R. F. *J. Phys. Chem. B* **1998**, *102*, 10650. (b) Angelomé, P. C.; Andrini, L.; Calvo, M. E.; Requejo, F. G.; Bilmes, S. A.; Soler-Illia, G. J. A. A. *J. Phys. Chem. C* **2007**, *111*, 10886.